

Recent Developments on a Simulator for Lunar Surface Operations

H. Nayar¹, A. Jain¹, J. Balaram¹, J. Cameron¹, C. Lim¹, R. Mukherjee¹,
M. Pomerantz¹, L. Reder², S. Myint¹, N. Serrano¹, S. Wall³

Jet Propulsion Laboratory, California Institute of technology, Pasadena, CA, 91109

New models and capabilities in the Jet Propulsion Laboratory’s (JPL) Lunar Surface Operations Simulator (LSOS) are reported in this paper. LSOS is a simulator built to support surface operations design and planning for future lunar missions. LSOS models surface systems, their mechanical properties, and operations. In addition to simulating the dynamic interactions during operations, for example, wheel-soil interaction or component motion, LSOS also models associated environmental, and system mechanical and physical processes. These include thermal, radiation and power transients, and terrain. Lighting models are used to generate material textures, reflectance and shadows. LSOS’s integrated architecture allows use of common models and enables interactions between components operating in different domains to be easily modeled. Models used in LSOS simulations and results from the simulation of two traverses are reported. The first is a replication of a traverse conducted during a field trial of prototype systems. The second is a traverse from a lunar outpost site near Shackleton Crater to Malapert Mountain. LSOS simulations and analyses will provide data to help in the optimization of mission plans.

I. Introduction

THE National Aeronautics and Space Administration (NASA) is leading an international partnership to develop and deploy a series of missions to return astronauts to the moon by 2025^[4]. In addition to habitation on, and exploration of the lunar surface, these missions, developed under NASA’s Constellation Program, will be precursors for subsequent manned missions to Mars. To enable these missions, new launch, crew transport, lander, and surface mobility vehicles and lunar habitat systems are being designed. NASA is performing studies of systems and operations planned for lunar missions in a series of field trials at lunar-analog sites on the Earth using prototype systems. Simulators are also playing a vital role in assisting in the mission design and planning, visualization and design optimization of these systems.

The Lunar Surface Operations Simulator (LSOS)^[15] is one of the simulators under development. As its name suggests, it models surface systems, their mechanical properties, dynamic interactions and operations. In addition to simulating the dynamic interactions during operations, for example, soil interaction or component motion, LSOS also models associated environmental, and system mechanical and non-mechanical processes. These include thermal, radiation and power transients, lighting and shadows, and terrain. LSOS’s integrated architecture allows use of common models and enables interactions between components operating in different domains to be easily modeled. For example, the illumination, solar panel power and thermal models use a common sun model and incidence angle. Simulations and post simulation analyses have been recently performed within LSOS to show that it can be a powerful tool to assist both in the design and planning of missions, and in component design optimization.

LSOS has been built on and extended from previous simulation packages developed at the Jet Propulsion Laboratory (JPL). Its core physics simulation engine is the DARTS package originally developed to simulate the Cassini spacecraft^[10]. DARTS is a multi-body domain-independent dynamics engine. Subsequent development around DARTS has led to supporting packages and simulators for a variety of space applications. These include Dshell^[3,14], SimScape^[13], ROAMS^[11,12], and DSEND^[2].

¹ Robotics and Mobility Section, 4800 Oak Grove Drive, Pasadena CA 91109.

² Flight Software and Data Systems Section, 4800 Oak Grove Drive, Pasadena CA 91109.

³ Strategic Planning and Project Formulation Office, 4800 Oak Grove Drive, Pasadena CA 91109.

New capabilities recently incorporated into LSOS and recently performed analyses and simulations are reported in this paper. The primary model components in LSOS that enable the lunar mission simulations are terrain and vehicle models. These are reported in Sections II and III respectively. In addition to dynamic simulation of mechanical components like vehicles driving over terrain, LSOS implements process dynamic models. These include power generation, storage and usage, communication signal strength, temperature and other processes that track variables of interest. Modeling and analyses of some of these elements is described in Section IV. Two long traverse sorties, a 3km field-trial traverse at Black Point Lava Flow in Arizona and a 570km traverse from Shackleton Crater to Malapert Mountain and back to Shackleton Crater near the South Pole of the moon, were simulated in LSOS. They are reported in Section V of this paper. We conclude in Section VI with a brief description of our on-going work and plans.

II. Terrain models

A. Field Trial Site at Black Point, AZ Terrain Model

The Black Point Lava Flow (BPLF) area is about 55 kilometers north of Flagstaff, Arizona. It features a large ancient lava flow field that is about 10 km by 15 km and is raised about 10 to 20 meters above the rest of the local terrain. The area was selected to approximate locations on the moon that feature transitions between different types of geography and rock and soil makeup. In order to perform vehicle simulations in the BPLF area, the USGS provided digital elevation maps (DEM) of a 30 by 25 km area surrounding the lava flow area from the USGS National Map Seamless Server. The DEM has a resolution of about 10 meters per posting. The original source of the DEM data is the National Elevation Dataset (NED). To complement the elevation data and provide a more realistic simulation, we procured digital imagery covering the same area. The imagery was purchased from a commercial vendor, but the original source of the imagery was the National Agriculture Imagery Program (NAIP). The resolution of the imagery is approximately 1 meter. To maximize the display and DEM resolution over the area to be traversed, given the large size of the texture image, we divided the area into an inset area and a context area. The inset area is 3 km square and has full DEM and image resolution. The context area (the rest of the area) has sub-sampled DEM data (by a factor of 4) and significantly sub-sampled imagery (by a factor of 8). A separate full resolution DEM was available for the entire area for vehicle dynamics computations. Figure 1 below shows the entire area and the inset area outlined in white.

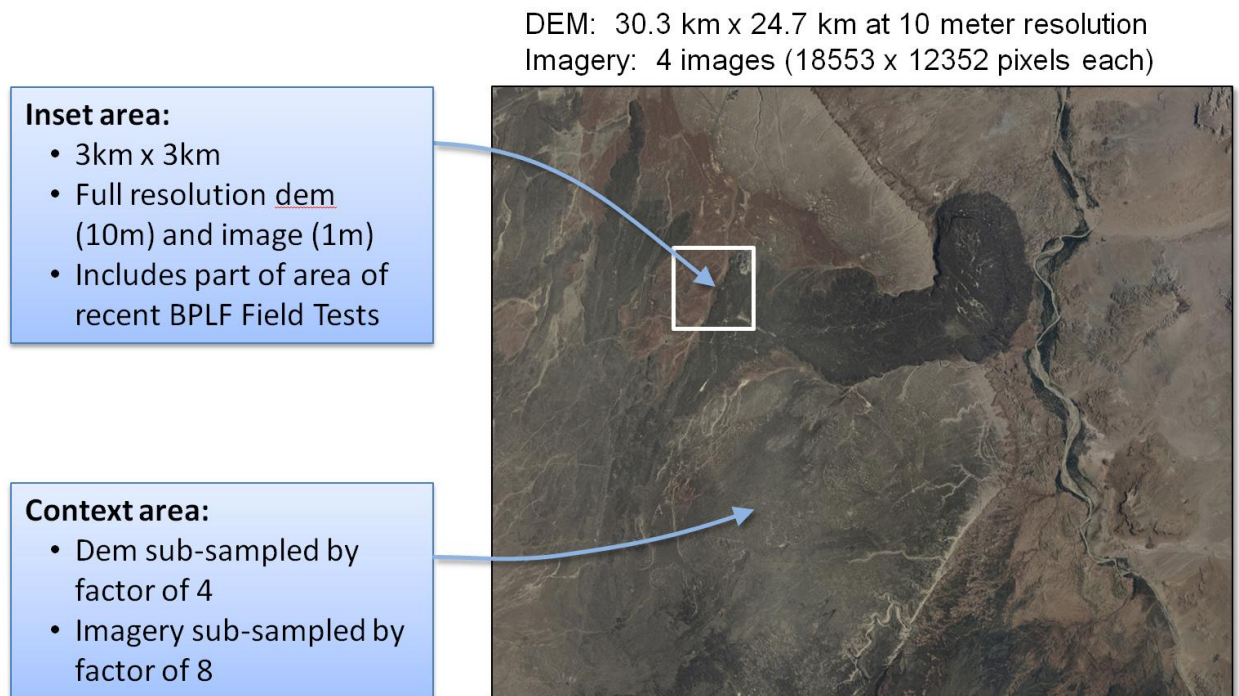


Figure 1: Black Point Lava Flow area

B. Goldstone Solar System Radar Lunar Terrain Model

There is significant interest in missions to the south pole of Earth's moon due to the fact that some locations near the Lunar South Pole are in sunlight most of the time^[6]. NASA's Jet Propulsion Laboratory has led efforts to collect elevation data near the Lunar south pole using large radar antennas at Goldstone, New Mexico. These are the same radar antennas that JPL uses for communicating with spacecraft in remote parts of the solar system. Several sets of data, called JPL Goldstone Solar System Radar (GSSR) data have been collected. The data that we used for LSOS was collected in 2006 and processed by USGS in 2008. The pixel spacing in the GSSR data is approximately 40 meters (although the accuracy is less than that in most of the area covered). This represented the highest resolution Lunar elevation data for this Lunar South Pole available at the time. The area covered is about 500 by 900 km.

The GSSR data has several issues. The primary and most problematic issue is that areas that are not visible from the GSSR antenna site have no elevation data. This includes bottoms of craters and areas behind mountains (as viewed from the Earth). There were other secondary issues with the GSSR due to radar data processing problems which led to a few artificial data artifacts such as bumps and dips in the data.

To create a terrain model of the GSSR data it was necessary to deal with large elevation data sets. In order to reduce the amount of elevation data LSOS had to deal with, we constructed an inset area and context area. The inset area is about 120 by 240 km and was sub-sampled by a factor of 4. The context area was sub-sampled by a factor of 20 to produce a terrain model with a manageable size. Since this time, LSOS has developed techniques to more effectively deal with larger data sets with constructing inset and context areas. We also filtered out some data in areas with large uncertainties in the underlying radar data. Figure 2 shows the full GSSR terrain model. Note that the south pole of the moon is near the intersection of the red lines. The inset area is outlined in white.

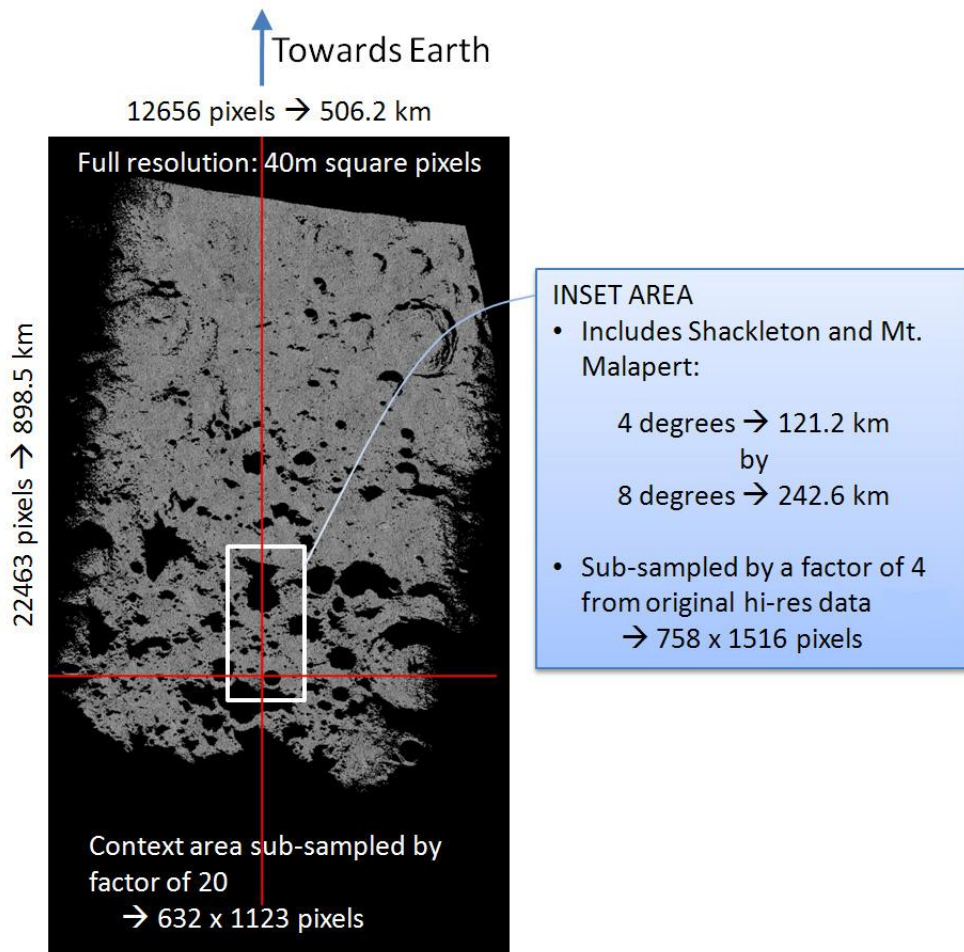


Figure 2: GSSR Terrain Model of Lunar South Pole

To give some feel for the traversability of the GSSR area near the South Pole, we constructed a slope map of the area surrounding Shackleton Crater (at the South Pole) (See Figure 3). Note that some of the odd slopes in the bottom left corner of the figure are due to data artifacts. The large black areas in the center of the crater and below the crater in the figure are black because of missing data, not because it is flat. This figure shows that the slopes on the interior of Shackleton crater are up to roughly 30 degrees. The slopes on the outside of the crater are between 20 and 30 degrees. Shackleton crater is about 19 km in diameter.

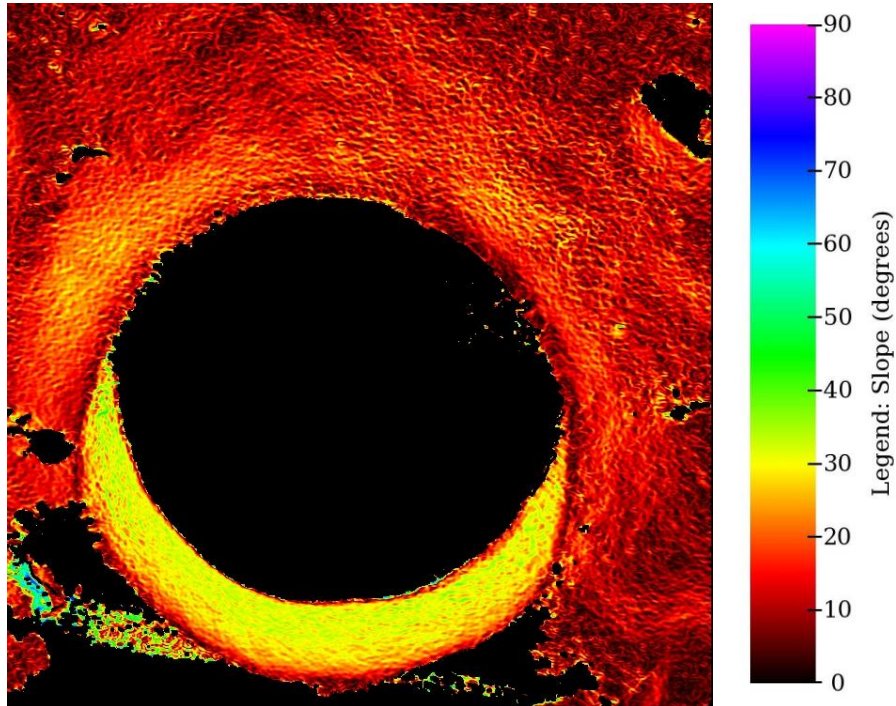


Figure 3: Slope Map of Shackleton Crater Area

III. Vehicle Models

The Lunar Surface Operations Simulator (LSOS) models various lunar vehicles such as the Un-pressurized Rover (UPR) and the Lunar Electric Rover (LER). The vehicle models in LSOS are built on the infrastructure developed in the ROAMS package at JPL. This allows for rapid vehicle model development using various re-usable modular software components from the ROAMS package. The vehicle models include high fidelity kinematics and dynamics of the vehicle, motors, encoders and controllers, interactions with the terrain as well as the ability to log various states of the system.

The mechanical aspects of the vehicle are modeled using $O(n)$ highly efficient recursive multi-body dynamics algorithms framework, called the Spatial Operator Algebra, developed over the last two decades at JPL^[18]. The underlying efficiency in the algorithms design enables high computational efficiency in modeling the kinematics and dynamics of the vehicles. The kinematics and dynamics of various components such as steered wheels, suspensions of various kinds, chassis dynamics, mast or arm motion, are accurately and efficiently modeled with faster than real time performance. The kinematics and dynamics of prescribed (controlled) and free (uncontrolled) joint motions are seamlessly captured in a unifying mathematical framework. Both joint accelerations and joint constraint forces can be calculated using these algorithms. The external or active forces and torques acting on the vehicles include lunar gravity, terrain interaction loads, and motor torques.

The interactions of the vehicle with the terrain are modeled using a physics-based wheel soil interaction model developed here at JPL. This model is based on the Terzaghi model and uses a Hunter Crossley spring damper model with tunable parameters to account for the interaction loads between the terrain and the wheels^[20]. Unlike the Terzaghi model, which is strictly static in nature, this model is a dynamic-equivalent where the time varying states of the spring damper model (deflection and rate of deflection) are used to model the interactions. This model

captures various essential physics of vehicle terrain interactions including slippage, rolling resistance, sinkage, various soil types and properties such as cohesion and spatially varying friction. The model has been validated using experimental testing on MER class rover on tilt-tables at JPL^[9]. For use on lunar terrain, the model is calibrated using lunar soil properties. In our studies, multiple simulations are used with parametric variations to generate a statistical measure of dynamic behavior rather than using a single simulation to produce a deterministic result.

The vehicle models feature physics-based actuator and sensor models. The wheel and steer motors are modeled as DC motors with damping and back EMF. The models are parametric in nature and different motors can be modeled by varying the motor characteristics such as armature resistance, current and torque constants. The sensor models are typically used to log the states of the system through IMUs and encoders. Full 3D visualization of the vehicles is enabled through VRML-based part graphics of various bodies in the system. The part graphics are articulated based on the kinematic model of the system, enabling realistic representation of the vehicle motion. Future enhancements on the vehicle models of the will include various additional physics-based models such as thermal models, power and battery models, models for charging from solar panels, and life support systems models.

The two primary vehicles modeled in LSOS are the Un-Pressurized Rover (UPR) and the Lunar Electric Rover (LER). Both these vehicles share the same underlying chassis, active suspension, steering and wheel models. Figures 4 and 5 show graphical representations of these vehicle models. Unlike previous MER class rovers, the UPR and the LER are much bigger vehicles with larger wheel-spans, active wishbone suspensions and a significantly larger chassis. Both vehicles are equipped with six wishbone suspensions. The wishbone suspension consists of three arms or links serially connected to each other and to the chassis by single degree of freedom rotational joints or pin joints. The axes of rotation of these joints are parallel to the chassis length. The upper link in the wishbone suspension is connected by a spring to the chassis. The system is equivalent to a planar four bar mechanism which is connected to the chassis by pin joints. As the vehicle moves over undulating terrain, the wishbone suspension articulates resulting in a restoring load through the spring which acts on the upper link and the chassis. The location of the spring mount on the chassis is adjustable, resulting in the ability to change the stiffness of the spring depending on the terrain. The wishbone suspension can also be actively controlled to raise or lower the chassis with respect to the ground.

The vehicles are equipped with steerable wheels connected through gearboxes. The gearboxes are treated as a lumped model i.e. a single gear models the total effect of the gear box. The constraint of the gearing law is accurately modeled. The steering of the wheels is enabled through the motion of a motor controlled single degree of motion rotational joint. The axis of rotation is in the vertical plane.

Two variations of the vehicle model are used in the LSOS. The Un-Pressurized Rover (UPR) is the unmanned vehicle and it consists of the mechanical system described above. The Lunar Electric Rover (LER) is the manned vehicle which shares the same vehicle architecture as the UPR. In addition, it is mounted with a cabin for the astronauts. The cabin is attached with body suits for the astronauts, which can be accessed from within the cabin. In our current vehicle model, the cabin and the body suits are modeled as extensions of the chassis with the assumption that they are rigidly attached to the chassis and there is no relative motion between the cabin and chassis.

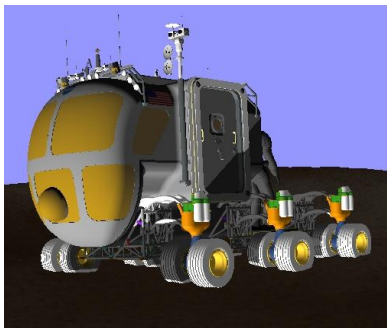


Figure 4. The LSOS Lunar Electric Rover (LER) model.



Figure 5. The LSOS Un-Pressurized Rover (UPR) model.

IV. Model Analyses

In addition to providing data on variables automatically tracked during the simulation, for example, distance traversed and vehicle speed, the following derived variables are also computed: power consumed, line-of-sight communication status to a base communication antenna and lighting and shadowing visualization. The procedures used to perform these analyses are described in this section.

A. Line of sight communication

Performing a line of sight determination can be computationally expensive when terrain and other vehicles or habitats can possibly obstruct the view from one communication sensor to another.

For a lunar rover simulation, line of sight communication is one of a variety of possible methods for communication between a lunar vehicle and habitat base station. By using the graphics card hardware-accelerated rendering capability of our Dspace visualization software^[17], we can perform these computations quickly and return accurate results back to the simulation.

During simulation setup, sensors that simulate communication antennas, are placed at specified locations on the LER vehicle and habitat. In addition, specifically colored “ornamental” geometry is placed at the same sensor locations for both the LER and habitat. These ornamental sensors are enabled for rendering only during line of sight computation and are not visible on-screen during the normal simulation run.

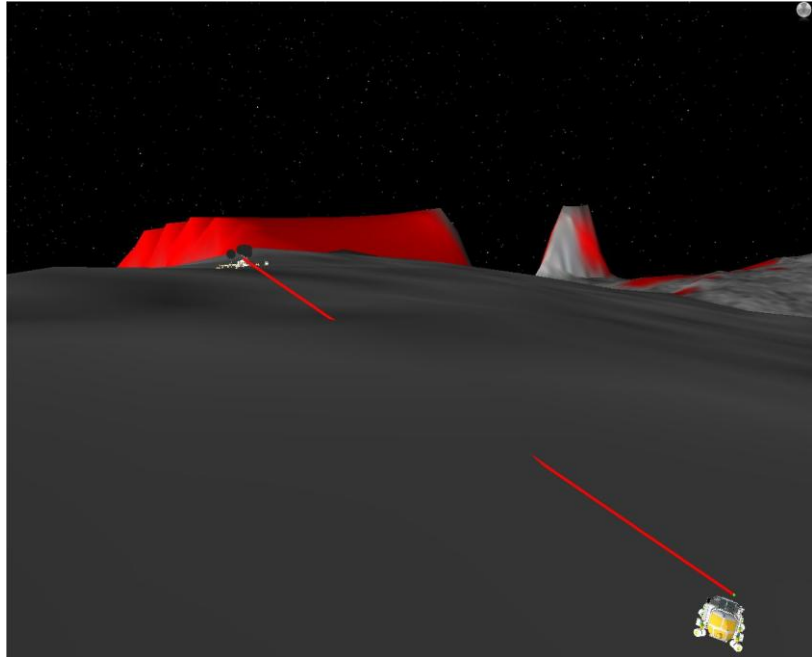


Figure 6. Terrain obstructed line of sight from LER vehicle to habitat

Using a multi-pass rendering technique, Dspace then renders the scene from the point of view of the LER vehicle sensor, looking at the habitat sensor. Scene renderings are maintained and processed in Dspace’s off screen memory. Pixel values at the center of each rendering are examined and if the previously specified sensor color is detected at the center of the each rendered image, point-to-point line of sight has been achieved and is reported to the simulation. If the specified color is not detected, it is assumed that a terrain feature, vehicle, or habitat component has obscured the view, as in the figure below, and a failed line of sight is reported to the simulation. Because we can perfectly control the camera placement and pointing during each of the two rendering passes, and for this initial implementation, assume point-to-point communication, we only need to examine pixels at the center of our rendered images and can achieve the desired results by rendering very small images, typically at a resolution of 32x32 pixels, which provides sub-second performance for line of sight calculation.

For testing, debugging, and to provide contextual information to the user, we often render a line segment between the two sensors under examination, as in the figure below, and color the line segment green or red depending on whether a pass or fail for line of sight has been achieved. This sensor-to-sensor line is for user information only, and is not part of the line-of-sight computation.

B. Lighting Models

The goal in the development of the lighting model was to build a simulation system that accurately determined the visual appearance of an LSOS scene given a particular terrain and lighting condition. The overall objective was to determine lunar surface appearance by implementing models for scene geometry, illumination and material reflectance properties. Phenomena modeled included direct illumination from the Sun and Earth, reflected illumination from terrain, artificial illumination, surface geometry, and surface reflectance physics as a function of both incident and reflected beam geometry.

The initial emphasis in the LSOS lighting model effort was to develop a generic capability of determining scene radiance that would be a building block towards determination of either a camera or a human-eye response. The model and associated rendering pipeline would operate upon the scene, lighting and radiosity models for a particular spectral frequency or frequency band. The obtained scene radiance could be used to determine both a "photo-realistic" rendering of the scene as well as a quantitative estimate of scene radiance levels, contrast, etc. Such a general capability could be used to determine the response of either a camera or the human eye by repeatedly invoking the model for multiple light frequencies or frequency bands (i.e. single-frequency "gray-level", 3 color channels, full visual spectrum, IR, etc.) and computing the appropriate weighted response integral (for either a camera or the eye) to determine the overall response required to determine appearance.



Figure 7. Example of Opposition Effect from Apollo.

Our initial implementation made the following simplifications:

- The Sun has an apparent magnitude of -26.7 and a full Earth as seen on the Moon has a brightness of -16.81^[19] (compared to a full Moon seen on Earth with an apparent magnitude of -12.7). The apparent magnitude of Venus is -4.7 and all other planetary bodies and stars are much dimmer. From this we see that the Earth can provide an illumination of about $1/10000$ of that of the Sun (i.e. $2.5 \text{ Log}[10000] = 10 \cong -16.8 - (-26.7)$) which is still a not insignificant value equivalent to that of about 44 full Moons (i.e. $2.5 \text{ Log}[44] \cong -12.7 - (-16.8)$) seen on Earth. However, all the other planetary bodies and stars have much lower apparent magnitude and their overall contribution is negligible compared to that of the Sun and the Earth. We therefore choose to model the natural illumination of only the Sun and the Earth and neglect all other celestial bodies.
- We propose to use simple Earth light-source model that neglects details of spatially varying albedo of the earth. Instead the light from the Earth would be modeled by a simple cosine function of the Sun-Earth-Moon phase angle.
- We make the approximation that the light from the Sun and the Earth can be modeled as a collimated, directional light source. This is a good approximation given the distance of the Sun and Earth from the lunar scene in comparison to other features in the scene. However, this approximation does not allow for the modeling of shadows with penumbras - a phenomena that could be important in low sun-angle conditions.
- We do not model transient phenomena such as dust.

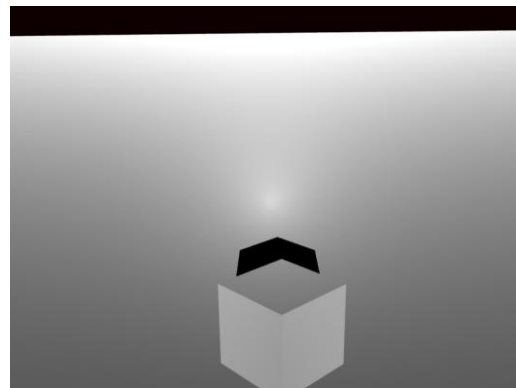


Figure 8. Opposition Highlight Effect and Shadows from Box-Shaped Object.

The lighting model was implemented using LSOS facilities and a *Rendering Engine* that works with the specified Shape and Material models. The *Rendering Engine* generates an image from a vantage point which is equivalent to determining the scene radiance. The *Rendering Engine* combines the *Blender*^[8] and *YafRay* open-source packages, because of their ability to meet the needs identified earlier.

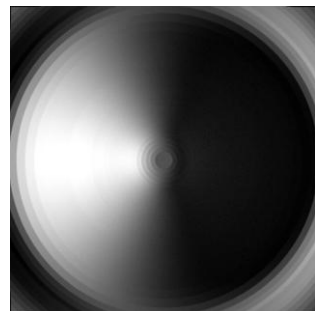


Figure 9 Radiance with Reflectance Function Incorporating the Opposition Highlight Effect

A set of experiments with both Lambertian and non-Lambertian models were conducted. The non-Lambertian cases with a model that incorporate opposition effects^[7] (see Figures 7 and 8) are shown here. This effect is important for Lunar surfaces and results in a highlight i.e. a bright spot in the image,

when the illuminant, scene and view are colinear. An example of such an effect is shown in Figure 7 from the Apollo-17 mission where we observe the brightened area surrounding the shadow cast by the astronaut.

We first illustrate the opposition effect for a planar terrain with a box (notionally representing the astronaut whose shadow is visible in Figure 7) casting a shadow onto a planar surface. All surfaces are modeled with a reflectance function incorporating the opposition effect. We deliberately choose a low albedo value of the LSO-BRDF as that provides the most pronounced opposition highlight effect. Unlike the scene with the astronaut where the view-point mostly coincides with the object casting the shadow, thereby placing the very low phase-angle illuminated terrain within the object shadow, we displace the view-point to be above the box so that the formation of the highlight at the zero phase-angle point is not hindered by the shadow points. The result is seen in Figure 8 where the highlight is clearly visible.

Lighting evaluations were also conducted with an analytic crater. The crater shape is modeled after typical craters observed on the lunar surface^[16]. The crater profile used had a deliberate factor of 4 vertical exaggeration to provide a deeply shadowed region in the crater. The result of rendering this crater is shown in Figure 9. Accurate visualization of the lighting conditions will help mission planners determine the need for artificial lighting and prepare lunar surface systems for the conditions astronauts will likely find when they arrive there.

C. Power

The Power Assembly is implemented using four *models*: a *Sun Angle Propagator model*, a *Solar Panel model*, a *Battery model* and a *Rover Power Consumer model*. A *model* in LSOS describes a component in the system dynamic model that has inputs, dynamic behavior that is described by parameterized difference or differential equations and has outputs. Outputs from one *model* may be used as inputs to another *model*.

The *Sun Angle Propagator model* uses the JPL SPICE Toolkit (See <http://naif.jpl.nasa.gov/naif/toolkit.html>) to track the sun position relative to the solar panel. Eclipses (earth blocking a portion of the sun) are currently not supported but may be implemented in a future version. Given the position of the sun and the orientation of the solar panel, the *Solar Panel model* computes the panel's output wattage based on the following parameters: incidence angle of the sun on the solar panel, sunlight intensity decay rate, and the maximum possible output wattage of the panel. The *Battery model* simulates the draining and charging of a battery. The *Solar Panel model's* output wattage is used as the input to the *Battery model* and the *Rover Power Consumer model* is connected to the *Battery's* output. The user can specify, using a parameter, the maximum battery level so the battery will not be charged beyond a certain limit. The *Rover Power Consumer model* estimates the power used by a rover. The *model* currently uses the following three formulas to estimate power consumption:

1. Power consumed by vehicle rolling resistance = rolling resistance (% of vehicle weight) \times horizontal velocity
2. Power consumed while driving up slopes = positive vertical component of velocity \times weight
Energy is not recuperated when driving down slopes in the model.
3. Standing still power consumption (a fixed parameter) that is also called the *hotel load*.

This simple model was found to capture the behavior of vehicle power consumption with sufficient accuracy when compared to actual traverses conducted by the LER vehicle in the field. During a simulation, the solar panels generate power, the battery stores excess power or provides power if power consumption is greater than power generation. The vehicle consumes power for driving and on-board processes. Incorporation of these models on a vehicle enables an integrated simulation that couples the vehicle motion to the power consumption model.

V. Traverse Simulations

In this section, we describe two simulations of traverses performed in LSOS. The first is a 3km traverse performed on the BPLF^[5] terrain model during a field trial exercise of the LER^[1] prototype. The second is a simulated traverse of a proposed lunar mission that starts near Shackleton Crater at the South Pole of the moon, drives to Malapert Mountain and returns to the starting location. This traverse replicates a scenario^[21,22] developed to optimize the science return from such a mission.

A. Black Point, AZ Field Trial Traverse

The simulation described in this section replicates a traverse conducted during field trial operations at BPLF in Arizona by the Surface Mobility Systems Team from the Johnson Space Center (JSC). The traverse selected for

simulation was the traverse performed on the first day of the field trial, Oct. 17, 2008, in initial checkout of the systems and vehicle. The traverse was at the edge of the lava flow and included driving on the lava flow and the sedimentary region below the lava outcrop. The path of the vehicle was provided by the field trial team collected using GPS. Figure va1 shows a plan view of the traverse path and Figure 11 shows a visualization at the end of the traverse and Figure 12 is a photo taken at the traverse site in Arizona.



Figure 10. Plan view of traverse path.

The vehicle model used in the simulation is the LSOS LER vehicle model. During the simulation, the vehicle was driven in velocity mode (specifying linear and angular velocity for the vehicle chassis) commanded using a manually controlled joystick. In the velocity mode, LSOS has an internal control algorithm that applies wheel steer angles and drive speeds corresponding to commanded chassis velocity. The vehicle was commanded to approximately follow the path taken by the actual vehicle based on traverse maps provided. The simulation start time was set to 17:00 on Oct 17, 2008 GMT and the traverse concluded at the simulation time of 17:56 on Oct 17, 2008 GMT. The integration step size used during the simulation was 100 milliseconds. Figure va2 shows the visualization of the LER vehicle model at the end of its traverse. Results from the traverse are listed on Table 1.

Time	56 minutes
Distance	2.90 km
Power consumed	5.374 kW-hr

Table 1. BPLF traverse data.



Figure 11. Visualization at the end of the BPLF simulation.

B. Shackleton Crater to Malapert Mountain and back to Shackleton Crater Traverse

A simulation of a traverse from a landing site on the moon near Shackleton Crater at the South Pole to Malapert Mountain, a site of science interest, and back to the starting location was also conducted in LSOS. The traverse is modeled on a suggested excursion proposed to conduct a science mission on the moon^[21,22]. Figure 13 shows the path for the traverse with thirteen waypoints specified along the path. These are locations where the vehicle stops for science activities. The GSSR terrain model was used for this simulation. The path for the simulation traverse was manually chosen to avoid areas with missing terrain data and steep and rough terrain. Areas with missing terrain data are shown in red on Figure 12. A time step of 100 milliseconds was used in this simulation.

The LER vehicle model was used for the traverse in the simulation. A list of navigation points defined the path to traverse. Navigation points were used to define the path to a higher resolution than waypoints in order to avoid hazards in the environment. An automatic algorithm was used to drive the vehicle. The algorithm commanded the vehicle to drive to the current navigation point. When within 3 meters of the navigation point, the vehicle was commanded to drive to the next navigation point in the list of navigation points and so on. The simulation time at



Figure 12. Photo of traverse site at BPLF, Arizona.

the start was 18:08 on March 21, 2021 GMT and the vehicle returned back to the start location at 22:32 on March 28, 2021 GMT. Results from the simulation are listed on Table 2 and a plot of energy consumed plotted against time is shown on Figure 14.

Time	172.4 hours
Distance	570.07 km
Power consumed	451.82 kW-hr

Table 2. Shackleton-Malapert traverse data.

VI. Conclusion

An overview of LSOS and preliminary results from simulations conducted with it are presented in this paper. We have developed a simulation environment for lunar surface operations that can generate data for use in designing systems and planning mission operations. As this capability is extended and ties to collaborating teams at other NASA centers and international partners are strengthened, LSOS will become an essential tool for the study and evaluation of future lunar mission surface operations scenarios.

Development continues on LSOS. New terrain models with higher resolutions will be developed to provide more realistic and accurate simulation results. As mission plans mature and component systems are defined in greater detail, new implementations of these surface assets will be modeled in LSOS to evaluate and predict their performance. Capabilities are also being developed in LSOS to simulate more complex scenarios involving multiple surface systems performing coordinated operations. In addition to extending the modeling and analysis capabilities, we are also working on the LSOS software infrastructure to improve simulation performance, handle larger and more complex models, and improve the visualization and analysis capabilities.

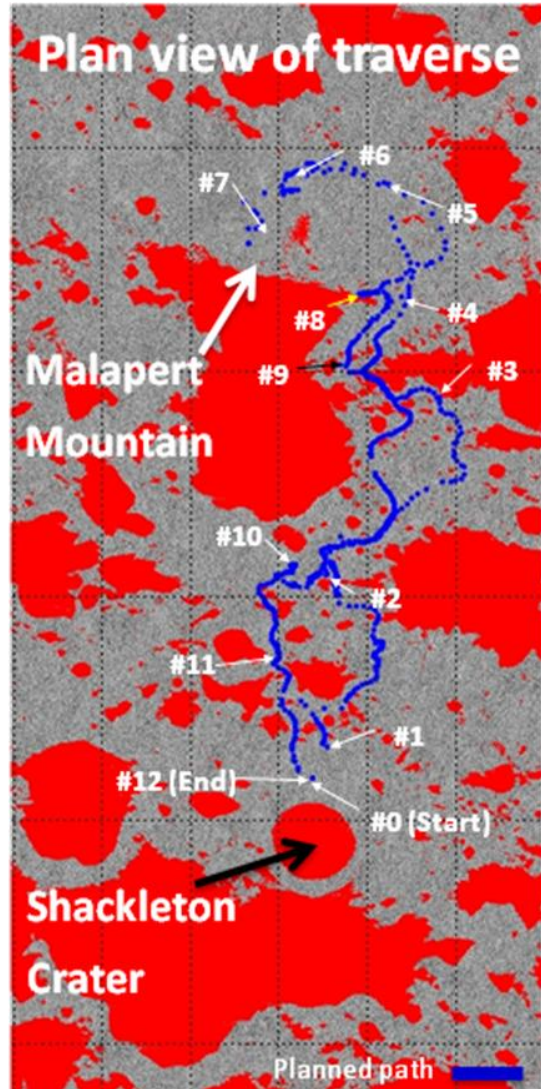


Figure 13. Shackleton-Malapert traverse.

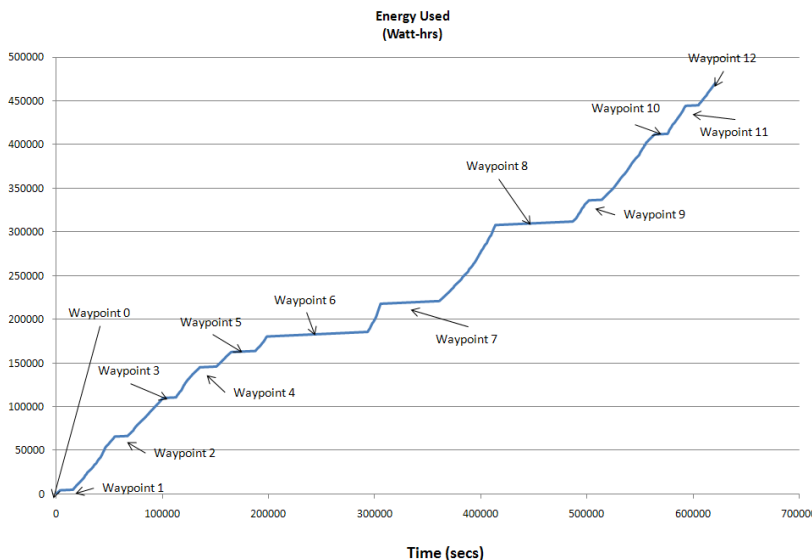


Figure 14. Energy consumed versus time for the Shackleton-Malapert traverse.

Acknowledgments

This work was carried out at the Jet Propulsion Laboratory, California Institute of Technology, under a contract with the National Aeronautics and Space Administration. We thank our sponsor, Doug Craig from NASA Headquarters, and our collaborators at the United States Geological Survey (USGS), NASA Glen Research Center, NASA Langley Research Center, NASA Johnson Space Center, NASA Ames Research Center, NASA Marshall Space Flight Center and Jet Propulsion Laboratory for support in the development of LSOS.

References

1. R. Ambrose, "Human-Robotics Interactions: Field Test Experiences from a collaborative ARC, JPL and JSC Team," *AIAA NASA 3rd Space Exploration Conference*, Denver, Colorado, February, 2008.
2. J. Balaram, R. Austin, P. Banerjee, T. Bentley, D. Henriquez, B. Martin, E. McMahon, and G. Sohl, "DSEDS - A High-Fidelity Dynamics and Spacecraft Simulator for Entry, Descent and Surface Landing," *IEEE 2002 Aerospace Conf.*, Big Sky, Montana, March 9-16, 2002.
3. J. Biesiadecki, D. Henriquez and A. Jain, "A Reusable, Real-Time Spacecraft Dynamics Simulator," in *6th Digital Avionics Systems Conference*, (Irvine, CA), Oct 1997.
4. D. Cooke, G. Yoder, S. Coleman, and S. Hensley, "Lunar Architecture Update," *AIAA NASA 3rd Space Exploration Conference*, Denver, Colorado, February, 2008.
5. W.B. Garry W. B., F. Hörz, G.E. Lofgren, D. A. Kring, M. G. Chapman, D. B. Eppler, J. W. Rice Jr., P. Lee, J. Nelson, M. L. Gernhardt, and R. J. Walheim, "Science Operations for the 2008 NASA Lunar Analog Field Test at Black Point Lava Flow, Arizona," *40th Lunar and Planetary Science Conference (2009)*, Texas, March 23–27, 2009.
6. J. Fincannon, "Lunar Polar Illumination for Power Analysis," *AIAA 6th International Energy Conversion Engineering Conference (IECEC)*, July 28-30, 2008, Cleveland, OH.
7. B. Hapke, *Theory of Reflectance and Emittance Spectroscopy*, *Topics in Remote Sensing*, Cambridge, 2005.
8. R. Hess, *The Essential Blender: Guide to 3D Creation with the Open Source Suite Blender*, No Starch Press, 2007.
9. T. Huntsberger, A. Jain, J. Cameron, G. Woodward, D. Myers, and G. Sohl, "Characterization of the ROAMS Simulation Environment for Testing Rover Mobility on Sloped Terrain" *International Symposium on Artificial Intelligence, Robotics and Automation in Space (i-SAIRAS 2008)*, (Hokkaido, Japan), August 30-Sept. 1, 2008.
10. A. Jain and G. Man, "Real-time simulation of the Cassini spacecraft using DARTS: functional capabilities and the spatial algebra algorithm," in *5th Annual Conference on Aerospace Computational Control*, (Jet Propulsion Laboratory, Pasadena, CA.), Aug. 1992.
11. A. Jain, J. Guineau, C. Lim, W. Lincoln, M. Pomerantz, G. Sohl, and R. Steele, "ROAMS: Planetary Surface Rover Simulation Environment," *International Symposium on Artificial Intelligence, Robotics and Automation in Space (i-SAIRAS 2003)*, (Nara, Japan), May 19-23, 2003.
12. A. Jain, J. Balaram, J. Cameron, J. Guineau, C. Lim, M. Pomerantz, and G. Sohl, "Recent Developments in the ROAMS Planetary Rover Simulation Environment," *IEEE Aerospace Conference*, March 2004.
13. A. Jain, J. Cameron, C. Lim, and J. Guineau, "SimScape Terrain Modeling Toolkit," *Second International Conference on Space Mission Challenges for Information Technology (SMC-IT 2006)*, Pasadena, CA, July 2006.
14. C. Lim and A. Jain, "Dshell++: A Component Based, Reusable Space System Simulation Framework," in *SMC-IT 2009*, Pasadena, CA, July 2009.
15. H. Nayar, J. Balaram, J. Cameron, A. Jain, C. Lim, R. Mukherjee, S. Peters, M. Pomerantz, L. Reder, P. Shakkottai, and S. Wall, "A Lunar Surface Operations Simulator." *Proceedings of the Simulation, Modeling, and Programming for Autonomous Robots 2008 (SIMPAN 2008)* : 65-74.
16. R. J. Pike. Apparent depth/apparent diameter relation for lunar craters. *Proc. Lunar Sci. Conf.* 8th. 1977. pp 3427-3436.
17. M. Pomerantz, A. Jain, and S. Myint, "Dspace: Real-time 3D Visualization System for Spacecraft Dynamics Simulation," in *SMC-IT 2009*, Pasadena, CA, July 2009.
18. G. Rodriguez, K. Kreutz-Delgado, and A. Jain, "A Spatial Operator Algebra for Manipulator Modeling and Control," *The International Journal of Robotics Research*, vol. 10, pp. 371-381, Aug. 1991.
19. R. W. Schmude. Full-Disc Wideband Photoelectric Photometry of the Moon. *J. Royal. Astr. Soc. Canada*, vol. 95. 2001. pp. 17-23.
20. G. Sohl and A. Jain, "Wheel-Terrain Contact Modeling in the Roams Planetary Rover Simulation", *Proc. Fifth ASME International Conference on Multibody Systems, Nonlinear Dynamics and Control*, Long Beach, CA, September 2005.
21. C. R. Weisbin, P. Clark, J. Mrozinski, K. Shelton, A. Elfes, J. Smith, W. Lincoln, H. Hua, and V. Adumitroaie, "Relative Achievement of Science Goals as a Function of Mission Duration for Exploration to the Moon's Malapert Mountain," July 21–23, 2009, NASA Ames Conference Center, NASA Ames Research Center, Moffett Field, California.
22. C. R. Weisbin, J. Mrozinski, W. Lincoln, A. Elfes, K. Shelton, H. Hua, J. H. Smith, V. Adumitroaie, and R. Silberg, "Lunar Architecture and Technology Analysis Driven by Lunar Science Scenarios," *Systems Engineering Journal*, Vol. 13, Number 3, 2010.